SciencePG
Science Publishing Group

Radiation-Induced Changes in Structural Network in Patients with Nasopharyngeal Carcinoma

Yin Tian, Yi Zhao

Department of Biological Information, Chongqing University of Posts and Telecommunications, Chongqing, China

Email address:

zhaoyi12231223@163.com (Yi Zhao)

Abstract: Radiation therapy (RT) is the standard radical treatment for nasopharyngeal carcinoma (NPC), and has produced excellent effects in terms of survival rate [1, 2]. However, one of the serious complications gave rise by the RT is brain injury. Previous studies have found that RT could cause brain structural abnormalities on gray matter and white matter. Nevertheless, the RT effects on the network level should be further investigated. Herein, we explored changes on the structural network for patients with NPC induced by RT. The structural magnetic resonance data (sMRI) were used to investigate the structural network in 20 NPC patients after and before radiotherapy. After constructing the structural network, we examined the radiation-induced changes in topology properties of small world network using graph theoretical analysis. Our results found that both the before and after radiotherapy groups showed small world properties. Compared with the before radiotherapy (pre-RT) group, the after radiotherapy (post-RT) group had lower global and local efficiency, longer shortest path length, and less clustering coefficient. In addition, the hub regions in the post-RT group were significantly different from the pre-RT group. Our findings exhibited the architecture of network topology and information transfer efficiency became poor in post-RT group. We speculated radiation therapy might induce the differences. The results can provide a new perspective to explore and diagnose radiation-induced brain injury and evaluate the effect of radiotherapy.

Keywords: Nasopharyngeal Carcinoma (NPC), Radiotherapy, Voxel-Based Morphometry (VBM), Gray Matter, Small World Properties

1. Introduction

Nasopharyngeal carcinoma is an endemic disease and rare in most regions of the world. However, it occurs much more frequently in Southeast Asia and China. In Southern China, NPC is one of the most common malignant tumors and the incidence of NPC is approximately 30–80 per 100,000 per year [3]. Because of the special lesion location, nasopharyngeal carcinoma is not suitable for surgical treatment and radiotherapy play a crucial part in NPC therapy. However, brain damage caused by radiation therapy is a serious complication, which has a serious impact on the prognosis and quality of life of the patients. Thus, it is necessary to understand the effect of radiation therapy on brain structure and find neuroimaging biomarkers to facilitate clinical diagnose, treatment, and prevention.

Previous studies have found that radiation therapy for NPC resulted in temporal lobe necrosis [4, 5]. It is believed that at least three different types of pathophysiological mechanisms are affected by irradiation: cerebral microbleeds (CMBs), white matter (WM) and gray matter (GM) lesions in NPC patients after RT [6-8]. Some studies also discovered gray matter (GM) necrosis, Chan et al. [6] found that GM lesions were detected in 88% of the involved temporal lobes, which always demonstrated thinning of the cortex with an irregular or blurred gray–white matter junction. Peterson, et al. [9] also found GM necrosis in years after the completion of RT. Radiation therapy caused abnormalities in the grey matter and white matter of the patients with NPC, which involves not only temporal lobe regions but also other normal brain regions [10]. The delayed effects of radiation damaged a range of structures, including the nervous system, bone, major vessels, mucus membranes, pituitary and salivary glands, as well as increasing the risk of radiation-induced neoplasms [11]. The cortical thickness altered in different period (eg, acute reaction period (few days to few weeks), early delayed radiation period (1–6

months), and late delayed radiation period (6 months to few years)), and this alterations were dynamic [12]. In terms of functional connectivity, a prior study found that the RT might induce functional connectivity impairments in NPC patients, which resulted in the cognitive impairments, especially the attention alterations [13]. A recent DTI study found that fractional anisotropy (FA) values showed significant change in different period, these abnormalities were most severe within 6 months after radiotherapy, and different brain regions exhibited distinct rates of recovery thereafter [14]. Furthermore, the indices of DTI have significantly changed in the temporal WM [15, 16], as well as regions of normal- appearing WM beyond the target field. To date, for the small-world properties of brain structural networks in NPC patients, few studies focused on the difference between after radiotherapy group and before radiotherapy group. In the present study, we explored the differences of both networks, and evaluated the effect of radiotherapy on the architecture of network. Meanwhile, this study provided a new insight into the pathogenesis of radiation-induced structural damage in brain network.

The human brain was a huge, interconnected, complex network with extraordinary topological attribute. The characteristic for the architectures of such a network was an important topic in neuroscience, but also an important way to understand how the brain integrates and transfers the information. The definition of the structural connectivity of the human brain relied on the brain imaging techniques from different modalities, such as morphological connectivity (GM volume, GM density, the thickness of the cortex and so on) based on structural magnetic resonance imaging (sMRI), and white matter connectivity based on diffusion tensor imaging (DTI) and diffusion spectrum imaging (DSI). In this study, we used the morphological metric of gray matter volume based on sMRI to construct the brain structural network in 20 patients with NPC after radiotherapy (post-RT) who had received the radiotherapy and 20 patients with NPC before radiotherapy (pre-RT) who were newly diagnosed but not yet medically treated, and both the after and before radiotherapy groups came from the same patients. And then we adopted the graph theoretical approach to investigate the topological organization of the structural networks. The structural connectivity matrixes were constructed by computing the Pearson correlation coefficients between the gray matter volumes of every two brain regions. Finally, the post-RT group was compared with the pre-RT group with respect to the global and nodal network properties, the aberrant brain network topologies associated with RT were evaluated.

2. Results

After the construction of the structure network, we employed the graph theory to describe the topological properties of the network in two groups. In this paper, we mainly focused on the small-world attributes.

2.1. Small-World Properties of Gray Matter Network

In the sparse threshold range of 0.29-0.54 with 0.01 intervals, the clustering coefficients (γ) and absolute path lengths (λ) in both the pre-RT and post-RT groups were calculated. As expected, both networks demonstrated small-world architectures (Figure 1) as the both networks had higher clustering coefficient ($\gamma>1$) and absolute path length ($\lambda\approx1$), and the sigma (σ) also above 1 ($\sigma=\gamma/\lambda$, $\sigma>>1$) over a wide range of sparsities ($0.29<S<0.54$) in comparison with the matched random networks. As the sparsity increased, γ and λ roughly decreased. In range of 0.29-0.40, the γ showing slight upward trend in pre-RT group, were smaller than that in post-RT group, but it was inverse in range of 0.41-0.54. The λ of both groups also decreased with the increase of sparseness, but the values of λ in pre-RT group were slightly larger than that in the post-RT group. The σ of both groups reduced with the increase of sparseness ($0.35<S<0.54$) and in most of threshold ($0.29<S<0.45$) the values of sigma in post-RT group were higher than that in pre-RT group.

The average shortest path length (L_p) and the average clustering coefficient (C_p) were shown in Figure 2. The values of L_p and C_p in both groups decreased with the increase of the sparsity ranging from 0.31 to 0.54. The L_p in the pre-RT group were shorter than that in the post-RT group. Compared to the post-RT group, the C_p of the pre-RT group were larger.

In the range of 0.29-0.54, the local efficiency (E_{loc}) and the global efficiency (E_{glo}) were calculated (Figure 3). As the sparse increased ($0.31<S<0.54$), the E_{loc} in both networks reduced. Specially, the E_{loc} in post-RT group were lower than that in pre-RT group. Instead, the global efficiency (E_{glo}) in both groups rose with the increase of sparsity and the global efficiency (E_{glo}) of post-RT were smaller compared to the pre-RT. As well known, the shorter the L_p of the network was, the higher the global efficiency. The greater the C_p was, the higher the local efficiency. Our results were consistent with the rules and demonstrated that with the intervention of radiotherapy, the network attributes of post-RT group revealed that the network topological structure got worse (decreased the global efficiency and the local efficiency).

2.2. Statistical Analysis

To compare the network metrics (L_p, C_p, γ, λ and σ) between the post-RT and pre-RT groups, one-way analysis of variance (One-Way ANOVA) ($p < 0.05$, uncorrected) were performed for each metric across the preselected sparsity ($0.29 \leq S \leq 0.54$) with intervals of 0.01, as shown in figure 4. There were significant differences in the L_p, C_p and λ between the post-RT and pre-RT groups ($p<0.05$). There were no significant differences in γ between the groups ($p=0.468$). Significant between-group differences were also observed in σ ($p=0.011$).

2.3. Hub Regions of the Two Grey Matter Networks

To ascertain the distribution of hub regions in the two grey matter networks, we calculated the normalized nodal betweenness centrality (B_i) of each node. If $B_i>$ mean+1.5SD [17] (mean represented the average of the normalized nodal

betweenness centrality, SD represented the standard deviation of the nodal betweenness centrality), the node i was considered as the hub node. In this study, when $B_i>3.88$, the node i was defined the hub node in pre-RT group. When the $B_i>3.07$, the node i was the hub bode in post-RT group. Based on our results, some regions were identified as hub regions in the cortical networks of each of the two populations. The details of the hub regions in the two cortical networks were shown in Table 1 and Figure 5.

In our work, the identified hub regions of the pre-RT group involved the right Parahippocampal gyrus (PHG), the left superior occipital gyrus (SOG), the right postcentral gyrus (PoCG), the right supramarginal gyrus (SMG), the left caudate nucleus(CAU), the right middle temporal gyrus (MTG). The left middle orbital frontal gyrus (ORBmid), the right inferior opercular frontal gyrus (IFGoperc), the right hippocampal gyrus (HIP), the right lingual gyrus (LING), bilateral supramarginal gyrus (SMG), the left superior temporal gyrus (STG), the right temporal pole (TPOmid) were included in the post-RT group. The right supramarginal gyrus was the hub region in the both groups. We could find some hub nodes in the post-RT group became non-hub nodes in pre-RT group, and other non-hub nodes of post-RT group converted into the hub nodes of pre-RT group. Although a few nodes were the hub in both groups, the nodal betweenness centrality altered. We inferred that these changes might be triggered by radiation therapy.

2.4. Changes in the Correlation Coefficients

Fisher's Z transformation was used to explore the between-group differences in the correlation coefficient. The significantly different correlation coefficients detected in pre-RT and post-RT groups ($p<0.01$) were shown in Figure 6. Regions that showed significant changes in the correlation coefficient between two groups primarily included the right inferior parietal (IPL), the right paracentral lobue (PCL), and the left paracentral lobule (PCL).

3. Discussion

Gray matter, which primarily consists of neuronal cell bodies, was a major component of the central nervous system and could directly reflect the congnitive function in the brain [18]. Covariation of gray matter volume might provide additional insight into the topographical organization of multiple cortical regions, previous studies adopted gray matter volume as an important measurement. Mechelli et al. [19] explored the covariation in the gray matter density between some regions of the brain to investigate brain symmetry, the researchers speculated that this covariation might be related with white matter fiber tracts (corpus callosum), and they suggested that covariation might be the result of mutually trophic influences or common experience related plasticity and the level of covariation might be disrupted in some patient populations. Montembeault et al. [20] analyzed the gray matter structure network in early stage of Alzheimer's Disease and found that the topology

architecture of the network altered. Zhu et al. [21] applied the gray matter volume network to examine the effect of age.

In this study, we constructed cortical networks of pre-RT and post-RT groups by calculating Pearson correlation coefficients between pairs of gray matter regions. And then, we mainly examined whether brain RT affected structural network properties in NPC patients. Finally, we applied graph theory to gray matter network estimates of 20 NPC patients before and after RT. The results of this study showed that the characteristics of the cortical network in the post-RT patients displayed poor topology. In particular, both the pre-RT and post-RT groups all exhibited small-world properties. However, the post-RT group showed slightly lower global and local efficiency than the pre-RT group, suggesting a disruption of the brain network and a shift towards regular networks. At the nodal level, our findings revealed that the hub nodal characteristics in the post-RT group significantly altered in several regions compared with pre-RT group, mainly included the left Middle orbital frontal gyrus (ORBmid), the right inferior opercular frontal gyrus (IFGoperc), the right hippocampal gyrus (HIP), the right Lingual gyrus (LING), the bilateral Supramarginal gyrus (SMG), the left Superior temporal gyrus (STG), and the right Temporal pole (TPOmid). Furthermore, these hub regions of the cortical network in post-RT patients provided additional structural evidence to support the opinion that brain RT affected structural network properties, and we speculated these regions might be associated with the cognitive impairment in post-RT patients with NPC. Our results provided unequivocal evidence of topological alterations in the brain networks, and contributed to understand some possible pathophysiological mechanisms underlying RT.

3.1. Small-World Properties of the Two Networks

Both the post-RT and the pre-RT groups displayed small-world topology properties in the structural networks (Figure 1). The small-world network proposed by Watts and Strogatz included the features of high clustering and short path length [22]. Our findings provided further evidence that this characteristic of brain architecture was robust to developmental aberration or disease. At the same time, the results revealed economical properties (Figure 2) in both groups, which suggested that the brain network tended to process information efficiently at a low cost.

Although both groups showed small-world topology, the global and local efficiency decreased in the post-RT group. Therefore, we inferred a disruption of the brain network and a shift towards regular networks. Previous evidence suggested that the speed of information propagation and the synchronizability across distant regions was stronger in small-world networks than in regular networks [23]. Thus, the abnormalities in the small-world network might reflect a less optimal network topology in post-RT patients with NPC. Significant between-groups differences were found in the global network properties (L_p, C_p, λ and σ) except the γ, which suggested that the abnormalities in the small-world network was related to the disruptive integrity of the

whole-brain network rather than the specific brain regions. Taken together, our findings demonstrated that the radiotherapy might cause alterations to the network topology in post-RT group.
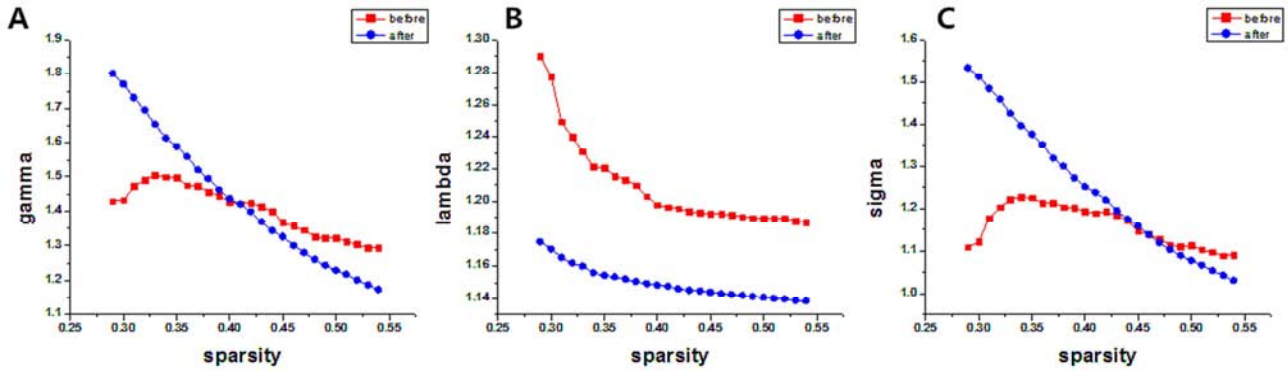

Figure 1. *Small-world properties of the structural cortical networks. The graphs show the absolute path lengths (gamma, $\gamma = C_p^{real}/C_p^{rand}$)), clustering coefficients (lambda, $\lambda = L_p^{real}/L_p^{rand}$) and the sigma ($\sigma = \gamma/\lambda$) over a wide range of sparsity values ($0.29 < S < 0.54$). All the networks have small-world properties ($\gamma > 1$, $\lambda \approx 1$, or $\sigma > 1$). As the values of the sparsity thresholds increase, the γ values decrease rapidly ($0.35 < S < 0.54$) and the λ values change only slightly. A – The values of gamma in before and after radiotherapy. B – The values of lambda in before and after radiotherapy. C– The values of sigma in before and after radiotherapy.*
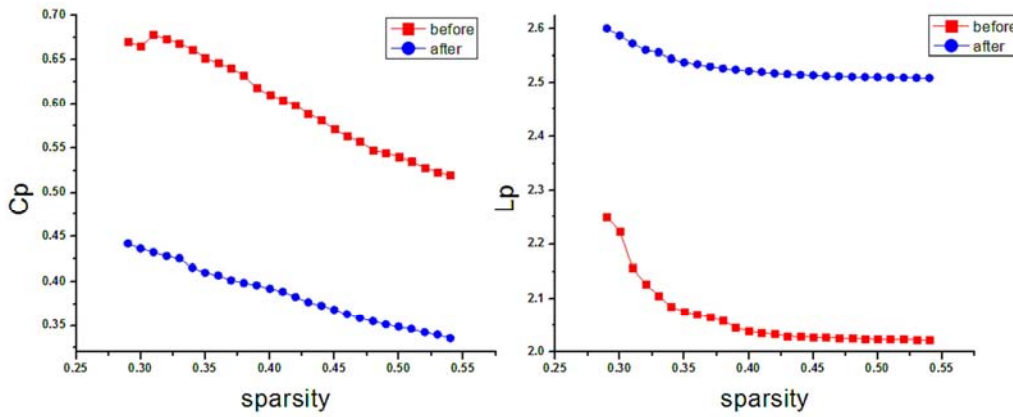

Figure 2. *Mean clustering coefficients and mean absolute path lengths of the cortical networks in the both groups. Mean clustering coefficient (C_p) and mean absolute path length (L_p) over a wide range of sparsity values ($0.29 < S < 0.54$). Left-picture: The red squares represent the mean clustering coefficient in the before radiotherapy (pre-RT) group. The blue circles represent the mean clustering coefficient in the after radiotherapy (post-RT) group. Right-picture: The red squares represent the mean absolute path length in the pre-RT group. The blue circles represent the mean absolute path length in the post-RT group. The mean clustering coefficient was greater for the pre-RT group and the mean absolute path length was shorter for the pre-RT group.*
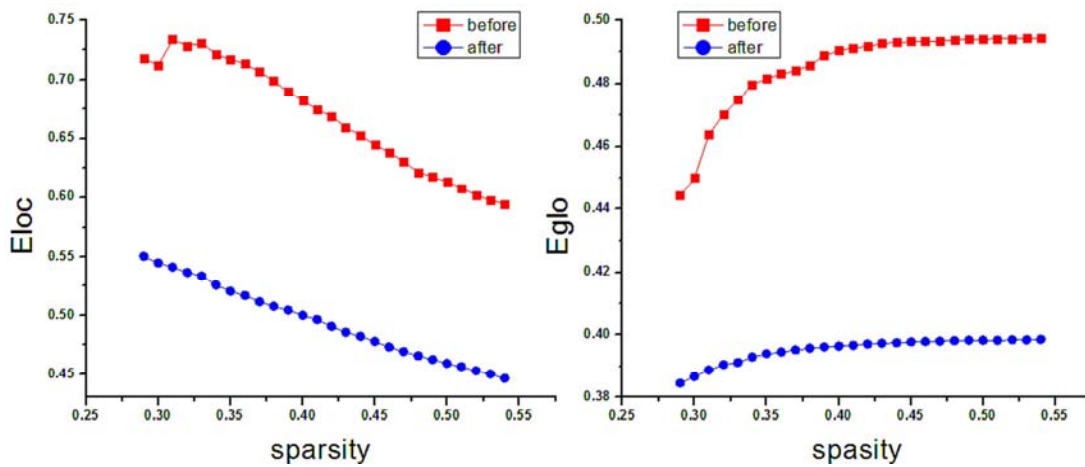

Figure 3. *Local efficiency (E_{loc}) and global efficiency (E_{glo}) of the cortical networks in the both groups over a wide range of sparsity values ($0.29 < S < 0.54$). Left-picture: The red squares represent the local efficiency (E_{loc}) of the patients before RT. The blue circles represent the local efficiency (E_{glo}) of the patients after RT. Right picture:-The red squares represent the global efficiency (E_{glo}) in the pre-RT group. The blue circles represent the global efficiency (E_{glo}) in the post-RT group. The local efficiency (E_{loc}) was greater for the pre-RT group and the global efficiency (E_{glo}) was higher for the pre-RT group.*
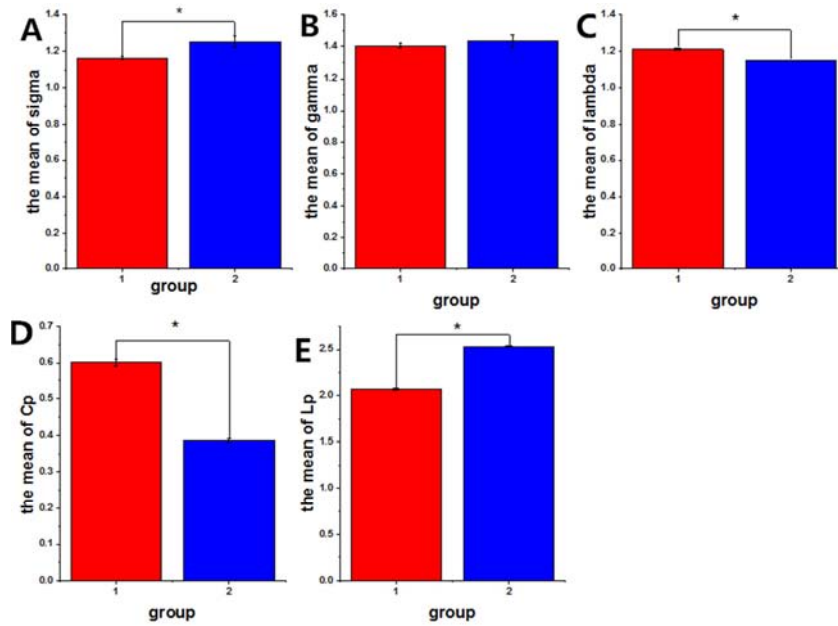
Figure 4. *The statistics analysis of the network attributes (One-Way ANOVA, p < 0.05). Red color: the patients before RT treatment. Blue color: the patients after RT treatment. the black star showed the difference between the two groups (p<0.05). A: There is significant difference between pre-RT and post-RT groups in sigma (p=0.011). B: there isn't significant difference between pre-RT and post-RT groups in gamma (p=0.468). C- pre-RT and post-RT groups have a significant difference in lambda (p=0). D- C_p was significantly different between pre-RT and post-RT groups (p<0.05). F-L_p was significantly different between pre-RT and post-RT groups (p<0.05).*
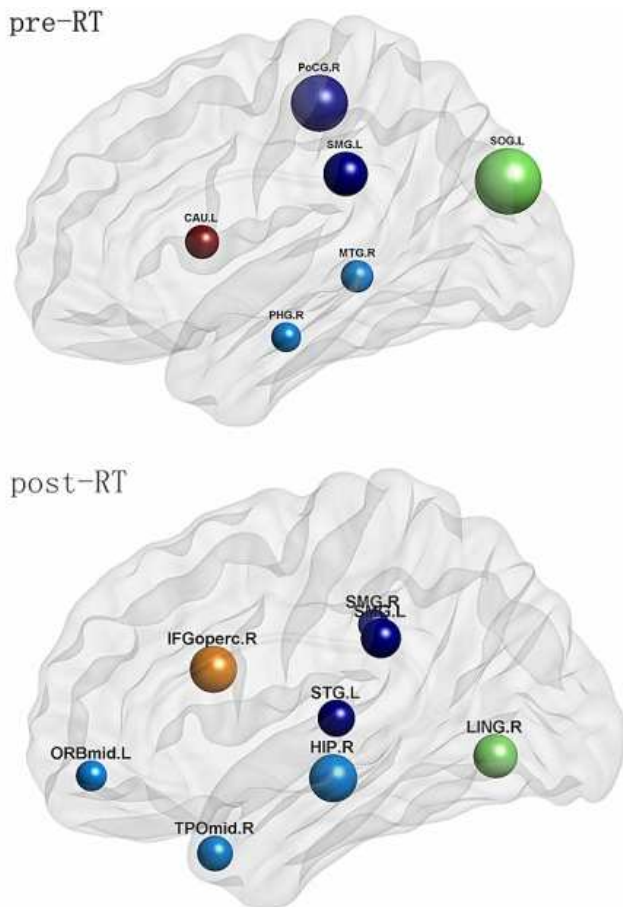

Figure 5. *The location of hub regions in the pre-RT and post-RT groups. Top picture: The hub regions in pre-RT group. Bottom picture：The hub regions in post-RT group. Note: the size of the spheres indicate the degree of nodal betweenness centrality.*
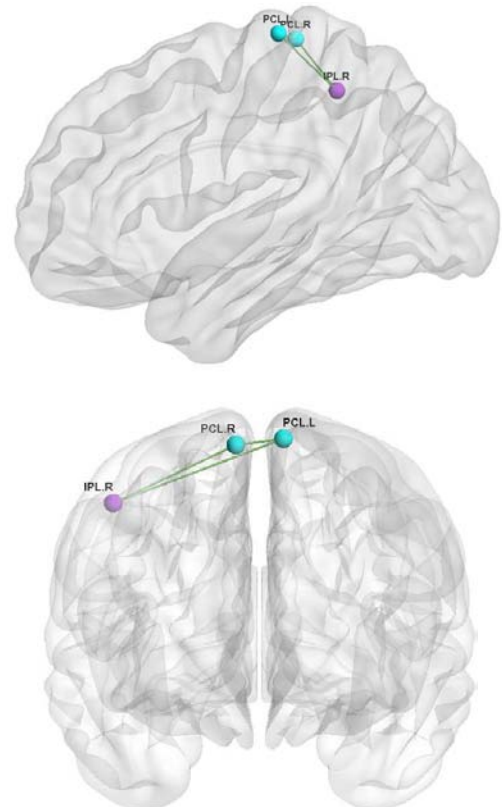

Figure 6. *The significantly different correlation coefficient between the pre-RT and post-RT groups. The line indicates that the interregional connectivity between pairs of regions has significant between-group differences (p<0.01, FDR-corrected).*

3.2. Hub Regions in Post-RT-Related Network

Hub node was a topological measure describing the

importance of a node for network organization [24]. To address the between-group difference, we considered the "betweenness centrality" of the nodes as a measurement of hub node in the networks. The nodal betweenness centrality estimates the influence of a node over information flow with the rest of the nodes in a network [25]. Using the measurement, we identified hub nodes in several brain regions in the both groups (Table 1), which indicated alterations in the activation of the regions. In particular, the hub regions in the pre-RT group were located in the right Parahippocampal gyrus (PHG), the left Superior occipital gyrus (SOG), the right Postcentral gyrus(PoCG), the left Supramarginal gyrus (SMG), the left Caudate nucleus(CAU), and the right Middle temporal gyrus (MTG). However, in the post-RT group, the hub regions mainly included the left Middle orbital frontal gyrus (ORBmid), the right inferior opercular frontal gyrus (IFGoperc), the right hippocampal gyrus (HIP), the right Lingual gyrus (LING), bilateral Supramarginal gyrus (SMG), the left Superior temporal gyrus (STG), and the right Temporal pole (TPOmid). Only the region of the right Supra Marginal gyrus (SMG) was the hub region in both groups, the rest of the hub regions were different between two groups.

Previous studies found that the radiation-induced functional impairments included the domains of short-term memory, language ability, list-generating fluency, attention, visual memory function, and motor abilities [26-28]. This study found that the hub regions were included the sensory-motor network, the visual network, the ventral attention network, the dorsal attention network, and the Emotional memory network [29-31].

The PHG, CAU, and HIP played important roles in the memory and emotional system [32-35]. In this study, the right PHG and the left CAU were the non-hub regions and the betweenness centrality of them decreased in post-RT group. The HIP was the hub node and the betweenness centrality of it increased in post-RT group. Those changed regions, located in the memory and emotional network, might related with the clinical manifestations of the memory of patients with NPC after radiotherapy. Studies showed that the radiation-induced functional impairments included the disorder of short-term memory [26], personality changes [36], a marked anterograde memory impairment for verbal material [37], and neuropsychological impairments in recent memory, immediate and delayed verbal recall and immediate visual recall [38].

The SOG and LING were the important areas in visual network [32-35]. The SOG was the hub node in post-RT group and the betweenness of it decreased compared with the pre-RT group. Those altered regions might reflect the impairments of visual function in post-RT patients, consisted with the clinical symptoms. The clinical study found that the patients with NPC who received radiotherapy had the disorder of visual [27], the impairment of higher-order visuospatial ability [38].

The MTG and STG located in ventral attention network [32-35], the MTG was the hub node in post-RT group, and the betweenness of the MTG decreased compared with the pre-RT. The STG was the hub node in post-RT group, and the

betweenness increased. The variation of those nodes might result in the attention ability injured. The prior study found that the post-RT patients shown the impairment of attention [26], neuropsychological impairments in the areas of auditory attention/concentration and immediate visual recall [38].

The PoCG played an important role in sensor-motor network [32-35]. The betweenness of the PoCG reduced in post-RT might trigger the damage of motor abilities of post-RT patients, which consisted with the clinical symptoms. Accumulated research demonstrated that the disorder of motor ability [28], the swallowing impairment [39], Olfactory information processing deficits [40], and the impairment in bimanual dexterity [38] in post-RT group.

Compared with pre-RT group, the changed nodal betweenness centrality in post-RT group might reflect that the radiation field not only included lesion location, but also widely involved the normal brain regions, which warned us that the evaluation for radiotherapy effects should consider the damage to normal brain regions, not only the degree of killing the cancer cell. Meanwhile, it was important to control the radiation field, the precise scope of radiation could greatly reduce the damage to the normal brain regions. As well known, Radiation damage was inevitable, but it was an important topic for us in the future to how to balance the relationship between curative effect and damage.

3.3. Altered Correlation Coefficient in Pre-RT and Post-RT

Table 1. *The hub regions in the two networks of the two groups.*

AAL areas		Betweenness centrality (Bi)	
		pre-RT	post-RT
Parahippocampal gyrus	R	4.6657	0.6065
Superior occipital gyrus	L	10.4312	0.4288
Postcentral gyrus	R	8.9150	0.7821
Supramarginal gyrus	L	6.9478	4.7518
Caudate nucleus	L	5.3288	0.9502
Middle temporal gyrus	R	5.0989	2.674
Middle orbital frontal gyrus	L	0.3874	3.093
Inferior opercular frontal gyrus	R	0	6.0124
Hippocampus gyrus	R	0	6.1710
Lingual gyrus	R	0.0083	5.5141
SupraMarginal gyrus	L	6.9478	4.7518
SupraMarginal gyrus	R	0	3.097
Superior temporal gyrus	L	0	4.2382
Temporal pole: middle temporal gyrus	R	1.9618	3.9649

The abnormal correlation coefficients in two groups were shown in Figure 6. Compared with the pre-RT group, the post-RT patients were found to show a significant decrease in their correlation coefficient, mainly in the right Inferior parietal (IPL), the right Paracentral lobu (PCL), and the left Paracentral lobule (PCL). We also observed that the locations of these involved regions were distributed within attention and sensory-motor networks, might related with impairment of attention and motor [28]. Studies found that the anterior IPL showed significant connectivity with paracentral gyri, and supplementary motor area, consistent with a role in sensorimotor processing [41], and this conclusion might support our inference that the significantly decreased correlations between IPL and PCL severely effected on the

topology of sensory-motor network, furtherly weakened the motor ability of patients with NPC after radiotherapy.

4. Materials and Methods

4.1. Participants

The total participants included 20 right-handed patients with nasopharyngeal carcinoma (NPC) (mean age 49.5 ± 10.5 years, age range 33- 75 years) after radiotherapy who had received radiotherapy (RT) and before radiotherapy who newly diagnosed and without radiotherapy treatment. All the patients without disease of other system came from the same group, including 15 males and 5 females.

4.2. MRI Acquisition and Image Assessment

The MRI images of the whole brain were obtained by rapid acquisition of T1 weighted sequences with a high-resolution three-dimensional magnetic Spin echo using a Siemens 1.5 T MR scanner. Scan parameters: TR=750ms, TE=11ms, FOV=75×75cm^2, flip angle =150°, the matrix size =256 × 192, voxel size =1.0×1.0×1.0mm^3, slice thickness 3mm, layer spacing 3.6, the continuous acquisition of 36 layers of images covering the whole brain.

Structural MRI images data (3D-T1) were preprocessed using the voxel-based morphometry (VBM) toolbox implemented in the Statistical Parametric Mapping software (SPM8). Firstly, the structural images were registered into the standard MNI space according to 12 radiation parameters. Secondly, the spatially normalized images were segmented into gray matter, white matter and cerebrospinal fluid using a priori tissue probability maps (TPM) provided by ICBM. Thirdly, the segmented gray images were smoothed with a smooth kernel of 8mm to remove the influence of noise and increase the validity of statistical tests of the posterior parameters.

4.3. Construction of Anatomical Connection Matrix

The key to the construction of the structural network was to define nodes and edges. In the present study, 90 brain regions of interest (ROIs) obtained from the AAL template were taken as nodes. Each ROI represented a node of the network. The edge was defined as the connection between two nodes. Then a 90 × 90 correlation matrix was constituted for each group by calculating the pearson correlation coefficients between the grey matter volumes of all pairs of ROIs. Therefore, a 90×90 matrix was obtained for each group respectively. The correlation matrix was then used to construct a structural network G (N nodes and K edges, N=90). Furthermore, the correlation matrices were thresholded into binary matrices with a threshold value T. For an N × N undirected graph G, if the edge e_{ij} was larger than the predefined threshold value T, the edge existed between i and j and set as 1, otherwise it did not exist and set as 0. Thus, the original coefficient matrix was turned into a binarized matrix. Moreover, if the same threshold was selected for the coefficient matrixes of two groups, the nodes and edges might be different and the networks topology

was also changed. Consequently, it was difficult to assess radiation treatment effect on the network topology attributes of different groups. Therefore, instead of selecting a single threshold, we employed a range of sparsity threshold from 0.29 to 0.54 with intervals of 0.01 to make sure that networks of two comparison groups had the same number of edges or wiring cost. Specifically, in this range, it could not only make the both networks fully connected, but also insure small-world properties of the networks. The sparsity S was defined as the ratio of total number of edges in a network to the maximum possible number of edges to make sure that networks from two comparison groups had the same number of edges or wiring cost, i.e., S=k/[n (n-1) /2] [25, 42].

4.4. Small-World Network Measurements

According to the graph theory, we calculated the topological properties and evaluated the structural connectivity organization with the graph theoretical network analysis (GRETNA) toolbox (https://www. nitrc.org/projects/gretna/) [43, 44]. In this study, we computed six global network properties (C_p, L_p, γ, λ, σ, E_{glob} and E_{loc}) and a regional nodal measurement (nodal betweenness centrality, b_i).

1) The clustering coefficient of a structural connectivity network is the average of the clustering coefficients (C_p) of all nodes:

$$C_p = \frac{1}{N} \sum_{i \in G} C_i \qquad (1)$$

Where C_i is the clustering coefficient of a node i (as shown in Equation 2), defined as the ratio between the number of existing connections among the neighbors of the node and the number of all possible connections in the subgraph G_i [45]:

$$C_i = \frac{E_i}{K_i(K_i - 1)/2} \qquad (2)$$

2) The mean shortest path length (L_p) of a network is the average of the shortest path lengths between all pairs of nodes:

$$L_p = \frac{1}{N} \sum_{i \in G} L_i \qquad (3)$$

Where L_i is the mean shortest path length of a node i, which is defined as:

$$L_i = \frac{1}{N-1} \sum_{i,j \in G, i \neq j} \min \left| L_{ij} \right| \qquad (4)$$

Where the min $|L_{ij}|$ is the minimal absolute shortest path length between node i and node j (i.e., the smallest number of edges traversed to get from i to j).

3) The normalized clustering coefficient (γ) of the structural connectivity network is defined as:

$$\gamma = \frac{C_p}{C_{random}} \qquad (5)$$

where C_p indicates the mean clustering coefficient and C_{random} represents the mean clustering coefficient of one hundred matched random networks that have the same numbers of nodes, edges, and degree distribution as the real network [22, 42].

4) The normalized characteristic path length (λ) is computed as follows.

$$\lambda = \frac{L_p}{L_{random}} \qquad (6)$$

where L_p denotes the shortest path length of the structural connectivity network, L_{random} indicates the mean shortest path length of 100 matched random networks.

If the following criteria of a real network is met: $\gamma > 1$, $\lambda \approx 1$, or the small-world scalar $\sigma > 1$ ($\sigma = \gamma/\lambda$), the network could be considered as a small-world network. In other words, the small-world network has a higher clustering coefficient and a similar path length compared to a random network [22, 46, 47]

4.5. Efficiency of Small-World Networks

Generally, the global efficiency E_{glo} and local efficiency Eloc were used to evaluate the network efficiency.

1) The global efficiency E_{glo} of a network is the inverse of the harmonic mean of the shortest path length between each pair of nodes [25, 42]:

$$E_{glo} = \frac{1}{N(N-1)} \sum_{i,j \in G, i \neq j} \frac{1}{\min|L_{ij}|} \qquad (7)$$

2) The local efficiency E_{loc} denotes the average of all the local efficiencies of the nodes in subgraph G_i:

$$E_{loc} = \frac{1}{N} \sum_{i \in G} E_{nodal}(i) \qquad (8)$$

Where $E_{noda}(i)$ is the nodal efficiency of a node i calculated as the following:

$$E_{nodal}(i) = \frac{1}{N-1} \sum_{j,k \in G} \frac{1}{\min|L_{jk}|} \qquad (9)$$

The shortest path length and the global efficiency measure the global transport ability of the network. The shorter the length of the shortest path is, the higher the global network efficiency and the faster information transmission rate between nodes.

4.6. Hub Regions of the Both Networks

The regional nodal properties can be characterized by a number of key measurements, including the nodal degree D_{egi}, nodal efficiency E_{nodal} and the nodal betweenness centrality b_i [25, 42]. The b_i described the central degree of a node in a network from the viewpoint of information flow and is defined as the fraction of all shortest paths in the network that pass through node i.

In this paper, the normalized betweenness centrality B_i was used to describe hub nodes. Normalized betweenness

centrality is defined as:

$$B_i = b_i / <B> \qquad (10)$$

Where b_i represents the betweenness centrality of the node i, and $<B>$ indicates the average of the betweenness centrality of all nodes. When $B_i > mean + 1.5SD$ [48], the node i is regarded as the hub node (mean: the average of the normalized betweenness centrality and SD: the standard deviation of the normalized betweenness centrality).

4.7. Correlation Coefficient Analysis

In order to test whether the correlation coefficient of the networks were significantly different between the pre-RT and post-RT groups, Fisher's z transformation was applied to convert the correlation coefficients to z values which were approximately normally distributed [18]. A z statistic was used to calculate the differences of z values between two groups ($p < 0.05$). A false discovery rate (FDR) test was performed ($p = 0.01$) [18].

5. Conclusion

Overall, we investigated the topology organization of brain structural networks in patients with NPC using sMRI (T1W) and graph theoretical approaches. Our results suggested that the post-RT patients with NPC and the pre-RT patients with NPC showed small-world properties, which provided further evidence for the presence of small-world characteristics in complex brain structural networks of the patients with NPC. Moreover, the decreased global and local efficiency and the altered nodal topology were detected in the post-RT patients, suggested that the radiotherapy could cause a serious impact on the topological properties of brain structural networks. The characters of structure network and node properties after RT could be considered as a factor to evaluate the effect of radiation therapy. Taken together, our results would provide novel insights into understanding the pathophysiology underlying radiation-induced changes. It was clear that this study we did could provide a new means for investigating brain injury induced by radiotherapy.

References

[1] Li Y. Neurosurgery and prognosis in patients with radiation-induced brain injury after nasopharyngeal carcinoma radiotherapy: a follow-up study. Radiation Oncology. 2013; 8(1):1-6.

[2] Wu X, Gu M, Zhou G, Xue X, Wu M and Huang H. Cognitive and neuropsychiatric impairment in cerebral radionecrosis patients after radiotherapy of nasopharyngeal carcinoma. Bmc Neurology. 2014; 14(1):10.

[3] Tang LL, Guo R, Zhou G, Sun Y, Liu LZ, Lin AH, Mai H, Shao J, Li L and Ma J. Prognostic value and staging classification of retropharyngeal lymph node metastasis in nasopharyngeal carcinoma patients treated with intensity-modulated radiotherapy. Plos One. 2014; 9(10):e108375.

[4] Chan AT. Nasopharyngeal carcinoma. Annals of Oncology Official Journal of the European Society for Medical Oncology. 2010; 21 Suppl 7(7):vii308.

[5] Ying S, Zhou GQ, Qi ZY, Li Z, Huang SM, Liu LZ, Li L, Lin AH and Ma J. Radiation-induced temporal lobe injury after intensity modulated radiotherapy in nasopharyngeal carcinoma patients: a dose-volume-outcome analysis. BMC Cancer, 13, 1(2013-08-27). 2013; 13(1):397-397.

[6] Chan YL, Leung SF, King AD, Choi PH and Metreweli C. Late radiation injury to the temporal lobes: morphologic evaluation at MR imaging. Radiology. 1999; 213(3):800-807.

[7] Chen W, Qiu S, Li J, Hong L, Wang F, Xing Z and Li C. Diffusion tensor imaging study on radiation-induced brain injury in nasopharyngeal carcinoma during and after radiotherapy. Tumori. 2015; 101(5):487.

[8] Shen Q, Lin F, Rong X, Yang W, Li Y, Cai Z, Xu P, Xu Y and Tang Y. Temporal Cerebral Microbleeds Are Associated With Radiation Necrosis and Cognitive Dysfunction in Patients Treated for Nasopharyngeal Carcinoma. International Journal of Radiation Oncology Biology Physics. 2016; 94(5):1113.

[9] Peterson K, Clark HB, Hall WA and Truwit CL. Multifocal enhancing magnetic resonance imaging lesions following cranial irradiation. Annals of Neurology. 1995; 38(2):237-244.

[10] Lv XF, Zheng XL, Zhang WD, Liu LZ, Zhang YM, Chen MY and Li L. Radiation-induced changes in normal-appearing gray matter in patients with nasopharyngeal carcinoma: a magnetic resonance imaging voxel-based morphometry study. Neuroradiology. 2014; 56(5):423-430.

[11] King AD, Ahuja AT, Yeung DK, Wong JK, Lee YY, Lam WW, Ho SS, Yu SC and Leung SF. Delayed complications of radiotherapy treatment for nasopharyngeal carcinoma: imaging findings. Clinical Radiology. 2007; 62(3):195-203.

[12] Lin J, Lv X, Niu M, Liu L, Chen J, Fei X, Miao Z, Qiu S, Li L and Huang R. Radiation-induced abnormal cortical thickness in patients with nasopharyngeal carcinoma after radiotherapy. Neuroimage Clinical. 2017; 14(C):610-621.

[13] Ma Q, Wu D, Zeng LL, Shen H, Hu D and Qiu S. Radiation-induced functional connectivity alterations in nasopharyngeal carcinoma patients with radiotherapy. Medicine. 2016; 95(29):e4275.

[14] Duan F, Cheng J, Jiang J, Chang J, Zhang Y and Qiu S. Whole-brain changes in white matter microstructure after radiotherapy for nasopharyngeal carcinoma: a diffusion tensor imaging study. European archives of oto-rhino-laryngology: official journal of the European Federation of Oto-Rhino-Laryngological Societies (EUFOS): affiliated with the German Society for Oto-Rhino-Laryngology - Head and Neck Surgery. 2016; 273(12):4453.

[15] Wang HZ, Qiu SJ, Lv XF, Wang YY, Liang Y, Xiong WF and Ouyang ZB. Diffusion tensor imaging and 1 H-MRS study on radiation-induced brain injury after nasopharyngeal carcinoma radiotherapy. Clinical Radiology. 2012; 67(4):340-345.

[16] Xiong WF, Qiu SJ, Wang HZ and Lv XF. 1H-MR spectroscopy and diffusion tensor imaging of normal-appearing temporal white matter in patients with nasopharyngeal carcinoma after irradiation: initial experience. Journal of Magnetic Resonance Imaging Jmri. 2013; 37(1):101–108.

[17] Matthews PM, Filippini N and Douaud G. Brain structural and functional connectivity and the progression of neuropathology in Alzheimer's disease. Journal of Alzheimers Disease Jad. 2013; 33(Suppl 1):S163-S172.

[18] Yao Z, Zhang Y, Lin L, Zhou Y and Xu C. Abnormal cortical networks in mild cognitive impairment and alzheimer's disease. PLoS Computation Biology. 2010.

[19] Mechelli A, Friston KJ, Frackowiak RS and Price CJ. Structural covariance in the human cortex. Journal of Neuroscience the Official Journal of the Society for Neuroscience. 2005; 25(36):8303.

[20] Montembeault M, Rouleau I, Provost JS and Brambati SM. Altered Gray Matter Structural Covariance Networks in Early Stages of Alzheimer's Disease. Cerebral Cortex. 2015; 26(6):2650.

[21] Zhu W, Wei W, Yong H, Xia A, Anstey KJ and Sachdev P. Changing topological patterns in normal aging using large-scale structural networks. Neurobiology of Aging. 2012; 33(5):899.

[22] DJ W and SH S. (1998). Collectivedynamics of 'small-world' networks. Nature, pp. 440-442.

[23] Strogatz SH. Exploring complex networks. Nature. 2001; 410(6825):268.

[24] Bullmore E and Sporns O. The economy of brain network organization. Nature Reviews Neuroscience. 2012; 13(13):336-349.

[25] Achard S and Bullmore E. Efficiency and Cost of Economical Brain Functional Networks. Plos Computational Biology. 2007; 3(2):e17.

[26] Hsiao KY, Yeh SA, Chang CC, Tsai PC, Wu JM and Gau JS. Cognitive function before and after intensity-modulated radiation therapy in patients with nasopharyngeal carcinoma: a prospective study. International Journal of Radiation Oncology Biology Physics. 2010; 77(3):722-726.

[27] Lam LC, Leung SF and Chow LY. Functional experiential hallucinosis after radiotherapy for nasopharyngeal carcinoma. Journal of Neurology Neurosurgery & Psychiatry. 1998; 64(2):259.

[28] Cheung M, Chan AS, Law SC, Chan JH and Tse VK. Cognitive function of patients with nasopharyngeal carcinoma with and without temporal lobe radionecrosis. Archives of Neurology. 2000; 57(9):1347-1352.

[29] Ho NF, Chong JSX, Hui LK, Koukouna E, Lee TS, Fung D, Lim CG and Zhou J. Intrinsic Affective Network Is Impaired in Children with Attention-Deficit/Hyperactivity Disorder. Plos One. 2015; 10(9):e0139018.

[30] Mccarthy H, Skokauskas N, Mulligan A, Donohoe G, Mullins D, Kelly J, Johnson K, Fagan A, Gill M and Meaney J. Attention Network Hypoconnectivity With Default and Affective Network Hyperconnectivity in Adults Diagnosed With Attention-Deficit/Hyperactivity Disorder in Childhood. Jama Psychiatry. 2013; 70(12):1329.

[31] Murty VP, Ritchey M, Adcock RA and Labar KS. Reprint of: fMRI studies of successful emotional memory encoding: a quantitative meta-analysis. Neuropsychologia. 2011; 49(4):695-705.

[32] Zielinski BA, Gennatas ED, Zhou J and Seeley WW. Network-level structural covariance in the developing brain. Proceedings of the National Academy of Sciences of the United States of America. 2010; 107(42):18191.

[33] Mesulam MM. From sensation to cognition. Brain A Journal of Neurology. 1998; 121 (Pt 6) (6):1013.

[34] Liao W, Mantini D, Zhang Z, Pan Z, Ding J, Gong Q, Yang Y and Chen H. Evaluating the effective connectivity of resting state networks using conditional Granger causality. Biological Cybernetics. 2010; 102(1):57-69.

[35] Jann K, Kottlow M, Dierks T, Boesch C and Koenig T. Topographic electrophysiological s ignatures of FMRI Resting State Networks. Plos One. 2010; 5(9):e12945.

[36] Oncology DO, Hospital QV, Candos and Quatre Bornes. Báo cáo khoa học: "Radiation Induced Temporal Lobe Necrosis in Patients with Nasopharyngeal Carcinoma: a Review of New Avenues in Its Management" doc. Gastrointestinal Endoscopy. 2007; 65(5):AB155.

[37] Parkin AJ and Hunkin NM. Memory loss following radiotherapy for nasal pharyngeal carcinoma — An unusual presentation of amnesia. British Journal of Clinical Psychology. 2011; 30(4):349-357.

[38] Hua MS, Chen ST, Tang LM and Leung WM. Neuropsychological function in patients with nasopharyngeal carcinoma after radiotherapy. Journal of Clinical & Experimental Neuropsychology. 1998; 20(5):684-693.

[39] Phua SY, Leow LP and Chan MFL. Delayed onset of swallowing impairment following radiotherapy for nasopharyngeal carcinoma (NPC). Asia Pacific Journal of Speech Language & Hearing. 2013; 9(1):33-39.

[40] Hua MS, Chen ST, Tang LM and Leung WM. Olfactory function in patients with nasopharyngeal carcinoma following radiotherapy. Brain injury: [BI]. 1999; 13(11):905-915.

[41] Zhang S and Li CS. Functional clustering of the human inferior parietal lobule by whole-brain connectivity mapping of resting-state functional magnetic resonance imaging signals. Brain Connect. 2014; 4(1):53-69.

[42] Latora V and Marchiori M. Efficient Behavior of Small-World Networks. Physical Review Letters. 2001; 87(19):198701.

[43] Wang J, Wang X, Xia M, Liao X, Evans A and He Y. GRETNA: a graph theoretical network analysis toolbox for imaging connectomics. Frontiers in Human Neuroscience. 2015; 9(386):386.

[44] Bernhardt BC, Bonilha L and Gross DW. Network analysis for a network disorder: The emerging role of graph theory in the study of epilepsy. Epilepsy & Behavior E & B. 2015; 50:162-170.

[45] Physical RE. Intensity and coherence of motifs in weighted complex networks. Physical Review E Statistical Nonlinear & Soft Matter Physics. 2005; 71(2):065103.

[46] Humphries MD, Gurney K and Prescott TJ. The brainstem reticular formation is a small-world, not scale-free, network. Proceedings of the Royal Society B Biological Sciences. 2006; 273(1585):503-511.

[47] Liu Y, Liang M, Zhou Y, He Y, Hao Y, Song M, Yu C, Liu H, Liu Z and Jiang T. Disrupted small-world networks in schizophrenia. Brain. 2008; 131(4):945-961.

[48] Sporns O, Honey CJ and Kötter R. Identification and Classification of Hubs in Brain Networks. Plos One. 2007; 2(10):e1049.